FAM83H regulates postnatal T cell development through thymic stroma organization

Ogan B[1,3], Forstlová V[2], Dowling L[2], Šímová M[1,2,3], Vičíková K[2], Novosadová V[2], Špoutil F[2], Červenková S[2], Procházková M[2], Turečková J[1], Fedosieieva O[2], Labaj J[2], Nickl P[1,2], Křížová K[2], Procházka J[1,2], Sedláček R[1,2] and Balounová J[1,2]*

[1]*Laboratory of Transgenic Models of Diseases, Institute of Molecular Genetics of the Czech Academy of Sciences, Vestec, Czech Republic*

[2]*Czech Centre for Phenogenomics, Institute of Molecular Genetics of the Czech Academy of Sciences, Vestec, Czech Republic*

[3]*Department of Cell Biology, Faculty of Science, Charles University Prague, Czech Republic*

**Correspondence: Jana Balounova (jana.balounova@img.cas.cz)*

Highlights

- *Fam83h*-deficient mice show multiple epithelial defects, but no obvious enamel defects
- *Fam83h* deficiency impairs lymphocyte development
- *Fam83h* deficiency impairs thymic epithelial cell maturation and thymus function

Abstract

Family of Sequence Similarity 83H (FAM83H/ SACK1H) is primarily expressed in epithelial cells, where it interacts with casein kinase 1 (CK1) and keratins to regulate cytoskeletal organization, cell proliferation, and vesicular trafficking. Mutations in *FAM83H* are known to cause amelogenesis imperfecta, highlighting its critical role in enamel formation. We generated *Fam83h*-deficient mice (*Fam83h*$^{em2(IMPC)Ccpcz}$, *Fam83h*$^{-/-}$) and mice lacking a part of the N-terminal CK1-binding domain (*Fam83h*$^{\Delta 87/\Delta 87}$). Consistent with other *Fam83h*-deficient models, these mice are subviable, smaller in size, and exhibit a sparse, scruffy coat, scaly skin, general weakness, and hypoactivity. Notably, both strains show impaired lymphoid cell development in early postnatal life. In the thymus, *Fam83h* expression is confined to thymic epithelial cells (TECs), and its deficiency in stromal cells results in disrupted thymic architecture and severe block in the expansion of DN3 (double-negative stage 3) T cells, ultimately leading to insufficient T cell production. Single-cell transcriptomic analysis reveals that *Fam83h*$^{-/-}$ cortical TECs (cTECs) express reduced levels of the TEC master regulator *Foxn1*, and several of its downstream target genes, suggesting a critical role for FAM83H and CK1 in cTEC maturation.

Keywords: FAM83H; Lymphocytes; Thymocytes; Thymic Epithelial cells; Thymic stroma; Immune dysregulation; CK1; Wnt/β-catenin signaling pathway

Abbreviations: FAM83H, Family of Sequence Similarity 83H; CK1, casein kinase 1, TEC, thymic epithelial cells; scRNA-seq. single-cell RNA-sequencing; FCM, flow cytometry, bone marrow, BM; DP, the double-positive ($CD4^+CD8^+$); DN, double negative ($CD4^-CD8^-$); MS, mass spectrometry

1. Introduction

The Family with Sequence Similarity 83 Member H (FAM83H, or SACK1H) plays a crucial role in enamel formation (1). The FAM83 protein family, comprising eight members, is evolutionarily conserved across vertebrates yet remains relatively uncharacterized. All members share a conserved N-terminal domain known as DUF1669 (domain of unknown function), while each possesses a unique C-terminal region of variable length, contributing to functional diversity (2). Most dominant mutations causing hypocalcified amelogenesis imperfecta (ADCAI) occur in exon 5 of *FAM83H*. These mutations, often nonsense or frameshift variants, result in truncated proteins that likely disrupt the functional C-terminus, suggesting a dominant-negative mechanism (3,5). FAM83H maps to chromosome 8q24.3 in humans (3), while its murine ortholog resides on chromosome 15 (6). FAM83H interacts with casein kinase 1α (CK1α) at its N-terminus and with keratins at its C-terminus, playing a key role in organizing keratin filaments by recruiting CK1α (7). Keratin filaments support mechanical stability of epithelial cells (7). FAM83H may also influence enamel formation through its effects on keratin organization and desmosome assembly, thereby impacting epithelial cell polarity (8). FAM83H is predominantly expressed in epithelial tissues such as the intestine, skin, and mammary gland. It is also expressed during embryonic development but appears to be absent in immune cells (9). To date, nearly 20 distinct mutations in *FAM83H* have been identified, mostly in association with ADHCAI (10). Additionally, FAM83H expression correlates with poor prognosis various cancers, (11), including squamous cell carcinoma (12), gastric carcinoma (13), and breast cancer (14). Beyond enamel defects, *Fam83h* deficiency in mice leads to broader physiological abnormalities (10). For example, Zheng *et al*. demonstrated that a knock-in mouse carrying the *Fam83h* c.1186C>T (p.Q396*) mutation - analogous to the human ADCAI *FAM83H* c.1192C>T variant developed forelimb swelling and inflammation (15).

Lymphocyte development, particularly T cell differentiation, begins with hematopoietic stem cells in the bone marrow that generate lymphoid progenitors (16). T cell precursors migrate to the thymus, a primarily epithelial organ, where they differentiate (17). The thymus is dynamically remodeled by incoming hematopoietic progenitors (18). Reciprocal interactions between hematopoietic and stromal cells (known as lymphoepithelial crosstalk) support the stromal cell maturation in two main types—cortical and medullary thymic epithelial cells (cTECs/ mTECs) which then provide signals needed for T cell development (18, 19). Specifically, cTECs coordinate the early stages of T cell development and positive selection (20), and mTECs mediate negative selection (21). Recent single-cell RNA-sequencing (scRNA-seq) studies have revealed unexpected TEC heterogeneity and provided new insights into their development and function under homeostatic conditions (22, 19). Multiple molecular pathways govern thymic development, with the Wnt/β-catenin signaling pathway increasingly recognized as essential (23). Notably, overexpression of β-catenin overexpression in TECs reduces thymic cellularity and TEC numbers, highlighting the importance of finely tuned Wnt signaling (24).

FAM83H has emerged as a potential regulator of the Wnt/β-catenin pathway (25). Kuga *et al.* reported that *Fam83h* deletion led to reduced Wnt/β-catenin activity, evidenced by decreased expression levels of CK1α, CK1ε, and β-catenin (26). Unengaged CK1α is proposed to function as a negative regulator of Wnt/β-catenin pathway (27).

The role of FAM83H in the immune system has not been previously studied. We demonstrate, for the first time, that FAM83H expression in stromal cells significantly affects lymphocyte production. In the thymus, *Fam83h* deficiency disrupts stromal cell architecture, impairs DN (double-negative) T cell expansion in the cortex, and results in severely reduced T cell output. The same outcome is observed in animals with a truncated form of Fam83h lacking part of the CK1-binding domain, suggesting a critical role of the Fam83h-CK1α interaction in T cell development. Additionally, *Fam83h*-deficient cTECs show elevated expression of circadian rhythm genes and reduced expression of the TEC master regulator *Foxn1* and its multiple downstream targets, suggesting a broader impact on TEC maturation and function.

In summary, FAM83H, in coordination with CK1, is essential for organizing the keratin cytoskeleton in thymic epithelial cells. This structural role together with the impact on TEC maturation supports proper thymic architecture and is critical for sustaining normal T cell development.

2. Results

2.1 *Fam83h* is expressed in epithelial cells across multiple tissues

Fam83h is enriched in epithelial cells of the gastrointestinal tract, skin, bladder, tongue, pancreas, and mammary gland **(Figure 1A)** (34). We detected *Fam83h* mRNA expression in multiple organs, with the intestine showing unexpectedly higher levels than ameloblasts. Additionally, low levels of *Fam83h* mRNA were observed in the spleen and bone marrow (BM) **(Figure 1B).**

2.2. *Fam83h*-deficient mice display a spectrum of epithelia-related phenotypic abnormalities

We generated *Fam83h*-deficient mice (*Fam83h*$^{em2(IMPC)Ccpcz}$, hereafter *Fam83h*$^{-/-}$) and mice lacking part of the N-terminal casein kinase 1 (CK1)-binding domain (*Fam83h*$^{\Delta 87/\Delta 87}$) **(Figures 1C, and S6A)**. Consistent with other *Fam83h*-deficient models, *Fam83h*$^{-/-}$ mice are subviable, smaller in size, and display a sparse, scruffy coat, scaly skin, generalized weakness, hypoactivity, and develop skin and bone lesions early in life **(Figures 1D, S1A, B, and D)**. Notably, these manifestations appeared early in life, with few animals surviving beyond 2-4 weeks of age **(Figure S1A, and S6B)**. Histological analysis revealed forelimb edema with neutrophilic and lymphocytic infiltration (**Figure 1D**). Although dental abnormalities were not observed, bone mineral density appeared reduced in *Fam83h*$^{-/-}$ mice based on pseudo color analysis of micro computed tomography (μCT) images (**Figure S1B, C**).

2.3 FAM83H modulates hematopoietic cell output

Unexpectedly, *Fam83h*$^{-/-}$ mice exhibited increased myeloid and decreased lymphoid cells in peripheral blood during early postnatal life, peaking at week 3 **(Figures 1E, S1E, and S6C)**. In animals surviving beyond week 3, this imbalance began to normalize by week 8 and returned to baseline by week 12. Flow cytometry (FCM) analysis of BM progenitors (weeks 1-3) showed that while erythroid and myeloid progenitors remained largely unaffected, lymphoid progenitor production was markedly reduced **(Figure S2).** Specifically, common lymphoid progenitors, which sit at the top of the lymphoid hierarchy, significantly decreased in the BM of

Fam83h$^{-/-}$ animals at week 3. This decline then extended to downstream B and NK cell progeny **(Figure S2)**.

2.4 *Fam83h* deficiency disrupts thymic architecture and impairs T cell production

The deficiency in lymphoid progenitors was even more pronounced in the thymus. Starting at week 2, *Fam83h*$^{-/-}$ mice exhibited significantly reduced thymic weight and relative thymus-to-body weight ratios compared to wild-type (wt) controls **(Figure 2A, and S6D)**. Reduced proliferation was evident in both thymic epithelial cells (TECs) and thymocytes **(Figure 2B)**.

Histological hematoxylin-eosin and immunofluorescence (IF) analyses revealed severely disrupted thymic architecture in *Fam83h*$^{-/-}$ animals. The cortical region was markedly thinner, and medullary regions were poorly defined **(Figures 2C, D, and S3A)**. TECs appeared more rounded, with fewer protrusions and an increased co-expression of keratin 5 and keratin 8, indicating impaired TEC differentiation and organization **(Figures 2D-F, and S3A, B)**.

2.5 *Fam83h* deficiency impairs proliferation of DN T cell progenitors in the thymic cortex

FCM analysis of thymocytes at postnatal week 3 revealed a dramatic reduction in the double-positive (DP, CD4^{+} CD8^{+}) thymocyte population in *Fam83h*$^{-/-}$ mice **(Figure 3A, S6E)**. While some mice retained near-normal DP frequencies, others showed a severe loss, with DP cells comprising as little as 4% compared to ~86% in wt controls **(Figure 3A)**. Among all subsets, DP cells were the most affected (**Figure 3A, B).** Ki67 staining confirmed a significant decrease in proliferation among double-negative (DN) thymocytes, particularly in DN3–DN4 stages, which normally undergo extensive expansion. Apoptosis rates, however, were not significantly altered across progenitor subsets **(Figure 3C).**

To determine whether lymphopenia originated from *Fam83h* deficient stromal cells or hematopoietic cells, we generated reciprocal BM chimeras **(Figure 3D)**. The results confirmed that *Fam83h*-deficiency in in stromal cells, rather than immune cells, was responsible for BM lymphopenia and impaired T cell development (**Figure 3D**, right panels).

2.6 Fetal hematopoiesis is intact in *Fam83h*$^{-/-}$ animals

As numerous thymic deficiencies arise during embryogenesis, we analyzed hematopoiesis in fetal liver (FL) and thymus at embryonic days E17.5 and E18.5 (47). No differences were observed in FL hematopoiesis and early T cell development was also intact at E17.5 (**Figure S4A**). Imaging techniques, including µCT and IF imaging at E18.5 and E17.5 respectively, revealed normal thymus formation, positioning, size and thymic architecture in *Fam83h*$^{-/-}$ embryos compared to *Fam83h*$^{wt/wt}$ littermates (**Figures S4B, C**).

2.7 Single-cell profiling reveals FAM83H-dependent regulation of cTEC identity

To assess the molecular impact of *Fam83h* deficiency in TECs, we performed single-cell RNA sequencing (scRNA-seq) on sorted cortical TECs (cTECs) from *Fam83h*$^{-/-}$ and *Fam83h*$^{wt/wt}$ mice at postnatal week 2. The sc-transcriptomic analysis confirmed the previously described heterogeneity of week 2 old cTECs, sorted as CD45^{-}EpCAM^{+}UAE^{-}Ly.51^{+} cells (35, 19). The identified clusters included mature cTECs, (expressing *Prss16, Psmb11, Krt8, Foxn1, Ccl25*), proliferative intertypical/ cortico-medullary junction TECs, which shared some markers of perinatal (*Syngr1,*

Cxcl12) and intertypical TECs (*Pdpn, Ly6a*), and showed higher S-phase score, and two smaller clusters expressing makers of mTECs. We assigned these two clusters as an mTEC-like cluster enriched in *Ccl21a* and *Krt5* and a minor subset of a few cells expressing *Aire*, likely representing mature mTECs. Additionally, a minute cluster of contaminating T cells was identified based on hematopoietic marker gene expression (*Cd3e*) **(Figures 4A, and S5A).**

We focused our differential expression analysis on the mature cTEC cluster enriched in *Foxn1* as well as its multiple target genes **(Figures 4B and S5B)**, *Fam83h*$^{wt/wt}$ cTECs (red) expressed key TEC regulators, including *Foxn1, Ccl21a, Psmb11, Ubd, Dll4, Bak1,* as well as genes involved in cell adhesion (*Ajap1*) and Wnt or Notch signaling (*Tcf7, Dlk2, Hes6*). In contrast, *Fam83h*$^{-/-}$ cTECs (blue) were enriched for transcripts involved in circadian rhythm regulation, such as *Per1, Per2, Per3, Cry1, Cry2, Clock*, and *Ciart* **(Supplementary Table 2, and Figure S5C)**. Among 338 genes enriched in wt cTECs (Nygen score >0.7, log2FC >1), 29 were identified as high-confidence *Foxn1* targets (from 450 genes in total, (36)) suggesting that *Fam83h*-deficient cTECs cannot activate the *Foxn1* transcriptional program efficiently and ultimately fail to differentiate. RT-qPCR analysis of sorted cTECs (*Fam83h*$^{-/-}$ / *Fam83h*$^{wt/wt}$) confirmed the downregulation of *Foxn1* (logFC; -0.77), *Psmb11* (-0.78), *Ajap1* (-0.79), and *Ccl21a* (-0.32) in *Fam83h*$^{-/-}$ cells **(Figure 4C)**. Conversely, *Ccl2, Per1,* and *Txnip* were upregulated, potentially reflecting alterations in TEC homeostasis, chemotaxis, circadian rhythms and oxidative stress, validating the scRNA-seq findings on bulk cTEC samples **(Figure 4C)**. Overall, these results demonstrate that FAM83H plays a crucial role in TEC development by regulating the genes necessary for cTEC identity, maturation, and function.

2.8 FAM83H is essential for CK1 association with the keratin cytoskeleton

Given the established role of CK1α (*Csnk1a1*)) in keratin cytoskeleton organization (8) and our findings of disrupted keratin-5 and keratin-8 architecture in *Fam83h*$^{-/-}$ TECs, as well as epithelial defects in *Fam83h*$^{-/-}$ and *Fam83h*$^{\Delta 87/\Delta 87}$ animals, we investigated whether the truncated FAM83H protein, which lacks the first 87 amino acids in its N terminal domain, binds to CK1α. Due to the scarcity of TECs, we used ileum epithelial lysates from *Fam83h*^{wtwt,} *Fam83h*$^{-/-,}$ and *Fam83h*$^{\Delta 87/\Delta 87}$ animals (2-3 weeks old) for co-immunoprecipitation (Co-IP) with anti-CK1 and anti-FAM83H antibodies, followed by mass spectrometry (MS) analysis. As shown in Figure 1B, ileum shows abundant expression of *Fam83h*. Co-IP with anti-FAM83H antibody confirmed the FAM83H–CK1α interaction in *Fam83h*$^{wt/wt}$ samples, which was absent in *Fam83h*$^{-/-}$ lysates **(Figure 5A).**

Additionally, samples from *Fam83h*$^{\Delta 87/\Delta 87}$ mice showed a substantially reduced FAM83H–CK1 interaction **(Figure 5B).** Co-IP using CK1α antibody corroborated these findings: the FAM83H–CK1α interaction was seen in wt lysates but not in those from *Fam83h*$^{-/-}$ **(Figure 5C)** and *Fam83h*$^{\Delta 87/\Delta 87}$ samples **(Figure 5D).**

IF imaging of thymic cortex revealed that in wt animals, CK1α localized to well defined vesicles, evenly distributed in the proximity of the cell membrane. In contrast, in the absence of *Fam83h*, CK1α distribution was more diffuse or aggregated in larger structures **(Figure 5E)**. Taken together, loss or mutation of FAM83H disrupts the CK1-keratin cytoskeletal network, potentially contributing to epithelial structural defects and signaling defects.

Discussion

To date, FAM83H has primarily been studied in the context of amelogenesis imperfecta AI (3) intracellular transport, cytoskeletal organization (8), and cancer (13). In this study, we uncovered a previously unrecognized role of FAM83H in lymphopoiesis and T cell development. Our data identify *Fam83h* as a critical regulator of epithelial integrity, thymic stroma architecture, thymic epithelial cell (TEC) maturation, and T cell development, acting through its scaffolding function with casein kinase 1 (CK1) and keratin cytoskeletal proteins. We confirmed *Fam83h* expression across multiple epithelial tissues, with unexpectedly high expression in the intestine, surpassing that in ameloblasts, where it was originally characterized (5). Surprisingly, expression was also detected in hematopoietic organs such as the spleen and bone marrow (BM), suggesting potential roles beyond classical epithelial biology.

The early lethality and widespread epithelial defects observed in *Fam83h*-deficient mice underscore its essential role in maintaining epithelial homeostasis, consistent with earlier findings (37, 1). These findings align with the report from Zheng *et al.*, who described perinatal lethality, skin lesions, inflamed digits, and reduced size in *Fam83h* mutant mice (15). However, the precise cause of lethality in *Fam83h*$^{-/-}$ mice remains unclear.

Notably, we did not observe any dental abnormalities, corroborating findings by Wang *et al.* (38). However, altered bone mineralization suggests potential structural and developmental roles for FAM83H, supporting its known involvement in epithelial-mesenchymal interactions.

Unexpectedly, *Fam83h* deficiency also caused pronounced changes in the hematopoietic system, which had not been shown before. Peripheral blood analysis revealed a skewing toward the myeloid lineage and reduced lymphoid output, peaking at 3 weeks of age. BM analysis demonstrated a pronounced reduction in common lymphoid progenitors and their B and NK cell progeny, implicating *Fam83h* in early lymphoid lineage commitment. One of the most striking findings was the severe thymic atrophy in *Fam83h*-deficient mice. *Fam83h*-deficient mice exhibited reduced thymus size, disrupted stromal architecture, and impaired T cell output. TECs displayed altered morphology, reduced proliferation and a failure to support proper thymocyte development. Flow cytometry analysis revealed a significant reduction in double-positive (DP) thymocytes largely driven by defective proliferation of double-negative (DN) progenitors, particularly at the DN3–DN4 stages, confined to the cortical subcapsular zone. This suggests that loss of ***Fam83h*** in cTECs is the primary driver of the thymic phenotype. Reciprocal BM chimera experiments confirmed the stromal origin of the hematopoietic defects, indicating that *Fam83h* functions in a non-hematopoietic, niche-dependent manner to support immune development.

Interestingly, fetal hematopoiesis, thymic organogenesis and stromal architecture appeared intact in *Fam83h*-deficient embryos, indicating that *Fam83h* is dispensable during embryogenesis but becomes essential postnatally, when the T cell production is boosted in the mouse. We hypothesize that in the postnatal thymus when the demand for robust T cell output increases following massive BM progenitor seeding, FAM83H becomes essential for sustaining epithelial function (39).

Single-cell RNA sequencing of TECs further revealed a loss of mature cTEC identity in *Fam83h*-deficient mice. Canonical cTEC genes were downregulated, while transcripts involved in circadian

rhythm and stress responses were upregulated. Importantly, expression of genes in Wnt and Notch signaling pathways was impaired, suggesting that FAM83H may influence TEC maturation through these key developmental pathways. Prior studies have demonstrated that FAM83H interacts with CK1 and modulates Notch signaling, further supporting this hypothesis, and, linking these pathways (40, 41).

Collectively, our data suggest that FAM83H is not only essential for epithelial cytoskeletal organization (8) but also for sustaining the transcriptional program necessary for TEC identity and function. Although *Fam83h* has not been classified as a core thymic gene, its expression pattern across epithelial datasets such as those by Bornstein et al. indicates a significant role in TEC biology (19). Complementing this, Park *et al*. demonstrated that shifts in TEC populations correlate with stages of T cell development, initially dominated by cTECs and later balancing between cTECs and mTECs as thymocyte maturation proceeds. This observation supports the model of thymic cross-talk, wherein reciprocal signaling between developing thymocytes and TECs promotes their mutual differentiation and function (42). Given that *Foxn1* expression is regulated by Wnt signaling (43), it is plausible that FAM83H indirectly modulates key pathways governing TEC function through Wnt pathway regulation.

We confirm that FAM83H is essential for the association between CK1α and keratin cytoskeletal proteins, consistent with previous findings (40). The loss of this interaction in *Fam83h*-deficient and Δ87 mutant mice likely contributes to structural defects in epithelial cells, including TECs.

These data also suggest that CK1α activity may be essential for hematopoiesis in the context of *Fam83h* deficiency. Previous studies have shown that altering Wnt/β-catenin signaling in thymic epithelium impairs embryonic thymus development (44), and it has been proposed that *Fam83h* deficiency may perturb Wnt/β-catenin signaling in epithelial cells (25, 45). Future studies should investigate whether *FAM83H* mutations contribute to epithelial or immune pathologies in human diseases, particularly those with congenital or early-onset manifestations. In conclusion, our study establishes *Fam83h* as a key regulator of thymic epithelial cytoskeletal integrity and a critical determinant of thymic and hematopoietic homeostasis. Through its role in scaffolding CK1 and organizing the keratin cytoskeleton, FAM83H supports the structural and functional competence of epithelial tissues, particularly those governing immune development. Its loss leads to widespread defects in epithelial morphology, signaling, and lymphoid cell production, offering new insights into congenital disorders with both epithelial and immune components.

5. Materials and Methods

5.1 Animals

C57BL/6 mice were housed in individually ventilated cages (Tecniplast) with free access to water and food (Altromin), Safe Select Fine bedding (Velaz), and environmental enrichment under a 12/12 light-dark cycle. The study complied with EU laws. Experiments followed the Czech Centre for Phenogenomics (CCP) Standard Operating Procedures.

Generation of *Fam83h*$^{\Delta 87/\Delta 87}$ and *Fam83h*$^{-/-}$ mice

In this study, *Fam83h* mutant mice (*Fam83h*$^{\Delta 87/\Delta 87}$) with a 119 bp deletion on exon 2 **(Figure S6A)** and *Fam83h* knockout (*Fam83h*$^{-/-}$) mice (CRISPR/Cas9 technology) were generated within the IMPC effort (28). In *Fam83h*$^{-/-}$, the whole protein-coding sequence was deleted **(Figure 1C)**. The location of gRNAs was guiding RNA 1 > 23 bp (7595 – 7617) and guide RNA 2 > 23 bp (12522 – 12544), which are located on exon 2 and exon 5, respectively, and were selected as the target site, are shown in **Figure 1C**. For genotyping, specific primers were designed (listed in **Supplementary Table 1**).

5.2 Relative mRNA Expression (RT-qPCR)

To investigate RNA levels in *Fam83h*$^{wt/wt}$ and *Fam83h*$^{-/-}$ mice for comparison, total RNA was extracted with Qiagen RNeasy Mini Kit (Cat# 74104) and Micro Kit (Cat# 74004), approximately 0.3 - 1 μg of RNA was used for cDNA synthesis (Thermo Fisher, RevertAid First Strand cDNA Synthesis Kit, Cat# K1621). Primers are listed in **Supplementary Table 2.**

5.3 Histological staining, Hematoxylin eosin (H&E), and immunofluorescence (IF)

Paraffin sections were prepared by fixing samples in 4% PFA for >24 hours, transferring to 70% ethanol, embedding in cassettes, and sectioning at 4–5 μm (thymus) or 6–8 μm (paws). Forepaw samples were decalcified in Osteosoft (~1 month). Slides were deparaffinized (Leica ST5010–ST5030), and antigen retrieval was performed in 10mM citric acid (pH 6) ~15 min. H&E staining was done using Leica ST5020 + ST5030. Images were acquired on a Zeiss Axioscan.Z1 and Leica DM3000 LED microscopes at 20x/40x magnifications and analyzed using ZEN 3.1 and Leica Application Suite V4.13 software.
For cryosections, thymi were embedded in OCT, snap-frozen, sectioned at 7–10 μm at -20°C, and stored at -20°C. Slides were warmed ~10-15 min at RT, and fixed in 4% PFA, permeabilized (0.2% Triton X, 10 min), blocked (2.5% BSA), and incubated with primary antibodies (listed in **Supplementary Table 3**) overnight. Secondary antibodies and DAPI staining were applied the next day. Slides were mounted with fluorescent mounting medium, dried, and imaged using a Nikon CSU-W1 confocal microscope equipped with a Prior automated stage controlled by NIS Element Software at 20x and 100x objectives. Confocal Z stacks were generated through the entire z-axis of thymus tissues. Image analysis was performed using NIS-Elements (with AI) 6.0.2.

5.4 Micro-computed tomography (µCT) analysis

Crania and paws were dissected and preserved in 4% PFA for at least 3 days, and scanned in Skyscan 1176 (Bruker, Belgium). NRecon 2.2.0.6 (Bruker, Belgium) was applied for reconstruction of virtual section. After fixation in 4% PFA, E18.5 embryos were stained with 25% Lugol's solution for 10–14 days and embedded in 2.5% low-melting-point agarose (Sigma-Aldrich) one day before scanning. Scan was provided in Skyscan 1272 (Bruker, Belgium). InstaRecon 2.0.4.0 (InstaRecon, USA) plug-in was applied for reconstruction of the virtual section. Reconstructed data were visualized in CTvox (Bruker) with custom pseudocolor scales, and volumetric analysis was conducted using CT analyzer 1.18.4.0 (Bruker).

5.5 Flow cytometry (FCM) & Sorting

5.5.1 Single cell suspension preparation

Thymocytes were released from thymi using mechanical dissociation through cell strainer, bone marrow (BM) cells were prepared by crushing femurs and tibias in mortar. Upon red blood cell (RBC) lysis using ACK, cells were resuspended in FACS buffer (2% FBS, 2mM EDTA, 10mM HEPES in HBSS without $Ca^{2+}Mg^{2+}$) and counted. For BM progenitor assays, RBC lysis and Fc blocking were omitted.

5.5.2 Thymic stromal cell isolation

The thymus was enzymatically dissociated in RPMI + 2% FBS, 1 mg/mL Collagenase D, 1 mg/mL Dispase, and 40 U/mL DNase I, cut into small pieces, and incubated at 37°C for 30 minutes while rotating, with pipetting every 5 minutes. Afterward, FACS buffer (5–10mL) was added, and suspension was filtered through a >100µm mesh into 15mL tubes, adjusted to 5mL with FACS buffer. Then, RBCs were lysed, and cells were counted. CD45+ cells were depleted using EasySep™ Human CD45 Depletion Kit II (StemCells Technologies, Cat# 18945). After separation, cells were stained with the antibody mixture for 30 minutes on ice, then centrifuged and resuspended in FACS buffer.

5.5.3 Blood sample processing

Blood samples were collected from the facial vein into EDTA-coated tubes. Following 2-3 rounds of RBC lysis, samples were centrifuged (400*g*, 10 min, 4°C). Cells were stained with a pre-mixed antibody cocktail containing Fc block for 20 minutes at 4°C, washed, and resuspended in a FACS buffer supplemented with counting beads. Immediately prior to analysis, Hoechst 33258 dye was added, and samples were acquired at high flow rate.

5.5.4 Antibody staining - extracellular

Samples were stained with antibody cocktails (**Supplementary Table 4**) containing Fc block for 20 minutes at 4°C in the dark. Then, cells were washed with FACS buffer and centrifuged at 400*g* for 5 minutes at 4°C. The pellet was resuspended in FACS buffer. For the BM progenitor assay, containing CD16/32 antibody, no Fc block was added. For the apoptosis assay, cells were stained and washed in Annexin binding buffer instead of FACS buffer.

5.5.5 Antibody staining - intracellular - Ki67 staining

Upon surface marker and viability staining (*Fixable Viability Dye eFluor™*), cells were fixed and permeabilized using the eBioscience Foxp3/transcription factor staining buffer set (Invitrogen #00-5523-00) according to the manufacturer's instructions, washed, and stained with anti-Ki67 or isotype control antibody for 20-60 minutes at RT in the dark. Then, cells were washed with a permeabilization buffer.

5.5.6 FCM data acquisition, sorting, and analysis

For absolute blood cell count analysis, 5 µL of counting beads (CountBright™ Absolute, Invitrogen, C36950) were added and acquired on Cytek® Aurora (5L 16UV-16V-14B-10YG-8R, Cytek Biosciences). Sorting was performed with BD FACSAriaTM Fusion (4L 6V-2B-5YG-3R, BD Biosciences) in a biosafety Class II Type A2 cabinet. Full details of panels and gating strategies are described in **Figures S7-S16**. Data were analyzed using FlowJo software v10.10 (BD Life Sciences).

5.6 BM chimeras

P2-P3 neonates (CD45.2) were irradiated with two X-ray doses (each 3.5Gy) split by a 4-hour window. 5×10^6 ACK lyzed whole BM cells from a congenic donor (CD45.1) were injected into liver in 25 µL of HBSS. Animals were observed daily, and engraftment was analyzed from peripheral blood at 3 weeks of age. Thymi and BM were analyzed for hematopoietic outcome at 3-4 weeks post-transplant.

5.7 Single-Cell RNA Sequencing

5.7.1 Single cTECs sorting

Thymic stromal cells were isolated from week 2-old *Fam83h*$^{wt/wt}$ and *Fam83h*$^{-/-}$ animals (see above). cTECs were identified as CD45- Ter119- EpCAM+ UEA- Ly.51+ cells and single-cell sorted into 384-well plates already containing 0.3 µL of lysis buffer (29) and 3 µL of silicone oil (100 cSt, Sigma-Aldrich), using the Formulatrix Mantis. As a negative control, a subset of wells received no sorted cells.

5.7.2 Generation of smart-seq3xpress libraries (scRNA-seq)

Smart-seq3xpress libraries were prepared following published protocol (29) involving reverse transcription and 14 cycles of PCR pre-amplification after sample storage at −80°C. Indexed libraries were generated by transferring cDNA into plates with dried primers, followed by Tn5 tagmentation and PCR amplification for 16 cycles. Libraries were purified using SeraMag and SPRIselect beads, quality-checked on a Fragment Analyzer, quantified by Qubit, and sequenced on an Illumina NextSeq 2000 with 2 × 109 bp paired-end and index reads.

5.7.3 Analysis of scRNA-seq Data

Alignment of Raw Data

The raw read files were processed with zUMIs (version 2.7.9e) (30), applying published parameters (29) and settings documented in the supplemental file (Smartseq3xpress_SS3x_manuscript_all.yaml). Reads were aligned with STAR (version 2.7.3a) against mouse genome GRCm38, using gencode.vM8 annotation. Several downsampled count matrices were created, and for downstream analyses, a range of 10,000–20,000 reads per cell was used.

Data Processing

Subsequent steps were carried out in Seurat (version 5.2.1) (31), focusing on 5′-end tagged reads. Reads mapping to spike-ins (ERCC and SIRV) were excluded, and cells were filtered based on quality metrics (e.g., gene count >1200, RNA count >2200, spike-in <12%, mitochondria <6%). SCTransform with glmGamPoi was used for normalization (32, 33). Dimensionality reduction and clustering were done using the first 30 principal components, UMAP, and a resolution of 0.8. For integration, 50-dimension CCA via the IntegrateLayers function was applied. Seurat objects were converted to h5ad format and uploaded to Scarfweb. Data is available at https://www.nygen.io.

5.8 Mass spectrometry (MS) analysis of ileum samples

5.8.1 Co-immunoprecipitation assay (Co-IP)

Dynabeads™ Protein G (Invitrogen, Cat# 10004D) and a specific lysis buffer (20mM Tris-HCl, pH 7.4; 150mM NaCl; 1% Triton X-100 with protease inhibitors) were used to immune-precipitate proteins from tissue lysates. Tissues were lysed using mechanical disruption and centrifuged, followed by pre-clearing with Dynabeads. Lysates were incubated with dynabeads coated with antibodies against Fam83h and CK1α (**Supplementary Table 5**), and immunoprecipitated proteins were processed for Western blot or MS. LC-MS analyses were conducted at the OMICS Core Facility, Biocev, Charles University (https://www.biocev.eu/en).

5.8.2 Protein Digestion

Protein-bound beads were treated with TEAB/SDC buffer, reduced with TCEP, and alkylated with chloroacetamide. Proteins were digested on-bead with trypsin overnight at 37°C. After centrifugation and acidification with TFA, SDC was removed using ethyl acetate extraction (29). The resulting peptides were desalted using C18 stage tips (30).

5.8.3 LC-MS 2 Analysis

LC-MS analysis was performed using a Nano reversed-phase column (C18) with mobile phase buffers A (water, 0.1% formic acid) and B (acetonitrile, 0.1% formic acid). Peptides were loaded onto a trap column for 4 minutes and eluted using a gradient from 4% to 35% B in 60 minutes. Peptides were ionized by electrospray ionization and analyzed on a Thermo Orbitrap Ascend. Survey scans of peptide precursors were conducted at 120K resolution, and tandem MS was carried out with HCD fragmentation. Ion count targets and dynamic exclusion were set for optimal analysis.

5.8.4 Analysis of MS data

Data were analyzed and quantified using MaxQuant software (version 1.6.10.43) (31) with a false discovery rate (FDR) set to 1% for both proteins and peptides, and a minimum peptide length of seven amino acids. MS/MS spectra were searched using the Andromeda engine against a Mus musculus database. Specific modifications included carbamidomethylation of cysteine, acetylation of N-terminal proteins, and oxidation of methionine. The "match between runs" feature was applied for data transfer and quantification, utilizing label-free algorithms. Data was processed using Perseus 1.6.15.0, with log-transformed data and missing values imputed using a normal distribution method. For each antibody and corresponding dataset, t-tests were used to perform comparisons, and the results were visualized using a volcano plot. Genes showing at least a twofold difference and a statistically significant p-value ($p < 0.05$) were highlighted. All analyses were conducted in R version 4.4.3.

5.9 Statistical Analyses

Statistical analyses were conducted using GraphPad Prism (version 9). Data are presented as mean ± standard deviation (SD) or standard error of mean (SEM), with biological replicates (mice or embryos). Group comparisons were performed using unpaired two-tailed **Student's t-test** for normally distributed datasets with two groups, for comparisons involving multiple groups or timepoints, **one-way** or **two-way ANOVA** was used. For FCM analyses, mean frequencies of cell subsets were compared across genotypes and developmental stages using ANOVA or t-tests, depending on experimental design. Significance was set at $p \leq 0.05$. The level of significance is indicated in figures as follows: p-values: ns ($P > 0.05$), *$P \leq 0.05$, **$P \leq 0.01$, ***$P \leq 0.001$, ****$P \leq 0.0001$. In Smart-seq scRNA-seq analyses, cluster-based comparisons (e.g., S-phase scoring, gene expression) were performed using Nygen software pipeline (ScarfWeb) with in-built statistical modules (https://scarfweb.nygen.io/). Sample sizes, independent experiments, and statistical tests are reported in **figure legends**.

Data availability statement

The scRNA-seq data analyzed in this study are deposited on Zenodo database (doi: 10.5281/zenodo.15436243) and are available without restrictions. The MS proteomics data has been deposited to the ProteomeXchange Consortium via the PRIDE (48) partner repository with the dataset identifier PXD064193.

Conflict of interest disclosure

The authors declare no conflicts of interest

Ethics approval statement for animal studies

The study complied with EU laws (Project licence AVCR 4212-2023 SOV II). Experiments followed the Czech Centre for Phenogenomics (CCP) Standard Operating Procedures.

Author contributions

Betul Ogan, Veronika Forstlová, Laura Dowling, Kristína Vičíková, Kamila Křížová, Sylvie Červenková, František Špoutil, Michaela Procházková, Jolana Turečková, Olha Fedosieieva, Juraj Lábaj and Jana Balounová performed the experiments. Petr Nickl prepared the *Fam83h*-defficient mouse strains. Vendula Novosadová analyzed the data. Betul Ogan and Jana Balounová wrote the manuscript. Jana Balounová, Jan Procházka and Radislav Sedláček designed and supervised the study and obtained funding. All authors approved the final manuscript.

Acknowledgments

This work was supported by *LM2023036* and **CZ.02.01.01/00/23_015/0008189** (*Upgrade of the large research infrastructure CCP III*), co-funded by the European Union and the Ministry of Education, Youth and Sports of the Czech Republic (MEYS). We also acknowledge previous support from the projects **LM2018126** (*Czech Centre for Phenogenomics*, MEYS) and **CZ.02.1.01/0.0/0.0/18_046/0015861** (*CCP Infrastructure Upgrade II*, MEYS and ESIF).

The authors acknowledge Imaging Methods Core Facility at BIOCEV, supported by the MEYS CR (**LM2023050** Czech-BioImaging), BIOCEV GeneCore Facility (https://www.biocev.eu/en/services/genecore-facility.7), and OMICS Mass Spectrometry Core Facility (Faculty of Science, Charles University) at Biocev research center for their support & assistance in this work.

References

1. Zhang Y, Yang J, Yao H, Zhang Z, Song Y. CRISPR/Cas9-mediated deletion of Fam83h induces defective tooth mineralization and hair development in rabbits. J Cell Mol Med. 2022 Oct 27;26(22):5670.

2. Fulcher LJ, Bozatzi P, Tachie-Menson T, Wu KZL, Cummins TD, Bufton JC, et al. The DUF1669 domain of FAM83 family proteins anchor Casein Kinase 1 isoforms. Sci Signal. 2018 May 22;11(531):eaao2341.

3. Kim JW, Lee SK, Lee ZH, Park JC, Lee KE, Lee MH, et al. FAM83H Mutations in Families with Autosomal-Dominant Hypocalcified Amelogenesis Imperfecta. Am J Hum Genet. 2008 Feb 8;82(2):489–94.

4. Ding Y, Estrella MRP, Hu YY, Chan HL, Zhang HD, Kim JW, et al. Fam83h is Associated with Intracellular Vesicles and ADHCAI. J Dent Res. 2009 Nov;88(11):991–6.

5. Lee SK, Lee KE, Jeong TS, Hwang YH, Kim S, Hu JCC, et al. FAM83H Mutations Cause ADHCAI and Alter Intracellular Protein Localization. J Dent Res. 2011 Mar;90(3):377–81.

6. Fam83h family with sequence similarity 83, member H [Mus musculus (house mouse)] - Gene - NCBI [Internet]. [cited 2024 Dec 25]. Available from: https://www.ncbi.nlm.nih.gov/gene?Db=gene&Cmd=DetailsSearch&Term=105732

7. Kuga T, Kume H, Kawasaki N, Sato M, Adachi J, Shiromizu T, et al. A novel mechanism of keratin cytoskeleton organization through casein kinase Iα and FAM83H in colorectal cancer. J Cell Sci. 2013 Oct 15;126(20):4721–31.

8. Kuga T, Sasaki M, Mikami T, Miake Y, Adachi J, Shimizu M, et al. FAM83H and casein kinase I regulate the organization of the keratin cytoskeleton and formation of desmosomes. Sci Rep. 2016 May 25;6(1):26557.

9. FAM83H protein expression summary - The Human Protein Atlas [Internet]. [cited 2024 Feb 4]. Available from: https://www.proteinatlas.org/ENSG00000180921-FAM83H

10. Song YL, Wang CN, Zhang CZ, Yang K, Bian Z. Molecular Characterization of Amelogenesis Imperfecta in Chinese Patients. Cells Tissues Organs. 2012 Mar 13;196(3):271–9.

11. Snijders AM, Lee S, Hang B, Hao W, Bissell MJ, Mao J. FAM83 family oncogenes are broadly involved in human cancers: an integrative multi-omics approach. Mol Oncol. 2017 Feb;11(2):167–79.

12. Tokuchi K, Kitamura S, Maeda T, Watanabe M, Hatakeyama S, Kano S, et al. Loss of FAM83H promotes cell migration and invasion in cutaneous squamous cell carcinoma via impaired keratin distribution. J Dermatol Sci. 2021 Nov 1;104(2):112–21.

13. Hussein UK, Ha SH, Ahmed AG, Kim KM, Park SH, Kim CY, et al. FAM83H and SCRIB stabilize β-catenin and stimulate progression of gastric carcinoma. Aging. 2020 Jun 20;12(12):11812–34.

14. Ríos-Romero M, Cedro-Tanda A, Peña-Luna M, Mancera-Rodríguez MA, Hidalgo-Pérez L, Cisneros-Villanueva M, et al. FAM83H-AS1 is a potential modulator of cancer driver genes across different tumors and a prognostic marker for ER/PR + BRCA patients. Sci Rep. 2020 Aug 24;10:14145.

15. Zheng X, Huang W, He Z, Li Y, Li S, Song Y. Effects of *Fam83h* truncation mutation on enamel developmental defects in male C57/BL6J mice. Bone. 2023 Jan 1;166:116595.

16. Kwon M, Kim BS, Yoon S, Oh SO, Lee D. Hematopoietic Stem Cells and Their Niche in Bone Marrow. Int J Mol Sci. 2024 Jun 21;25(13):6837.

17. Dik WA, Pike-Overzet K, Weerkamp F, de Ridder D, de Haas EFE, Baert MRM, et al. New insights on human T cell development by quantitative T cell receptor gene rearrangement studies and gene expression profiling. J Exp Med. 2005 Jun 6;201(11):1715–23.

18. Hirakawa M, Nagakubo D, Kanzler B, Avilov S, Krauth B, Happe C, et al. Fundamental parameters of the developing thymic epithelium in the mouse. Sci Rep. 2018 Jul 23;8(1):11095.

19. Bornstein C, Nevo S, Giladi A, Kadouri N, Pouzolles M, Gerbe F, et al. Single-cell mapping of the thymic stroma identifies IL-25-producing tuft epithelial cells. Nature. 2018 Jul;559(7715):622–6.

20. Takada K, Takahama Y. Positive-selection-inducing self-peptides displayed by cortical thymic epithelial cells. Adv Immunol. 2015;125:87–110.

21. Klein L, Kyewski B, Allen PM, Hogquist KA. Positive and negative selection of the T cell repertoire: what thymocytes see and don't see. Nat Rev Immunol. 2014 Jun;14(6):377–91.

22. Ishikawa T, Akiyama N, Akiyama T. In Pursuit of Adult Progenitors of Thymic Epithelial Cells. Front Immunol. 2021 Feb 25;12:621824.

23. Weerkamp F, Baert MRM, Naber BAE, Koster EEL, de Haas EFE, Atkuri KR, et al. Wnt signaling in the thymus is regulated by differential expression of intracellular signaling molecules. Proc Natl Acad Sci U S A. 2006 Feb 28;103(9):3322–6.

24. Swann JB, Happe C, Boehm T. Elevated levels of Wnt signaling disrupt thymus morphogenesis and function. Sci Rep. 2017 Apr 11;7:785.

25. Nasseri S, Parsa S, Vahabzadeh Z, Baban B, Khademerfan MB, Nikkhoo B, et al. CRISPR/Cas9-Induced Fam83h Knock-out Leads to Impaired Wnt/β-Catenin Pathway and Altered Expression of Tooth Mineralization Genes in Mice. Iran J Biotechnol. 2023 Oct 1;21(4):e3673.

26. Kuga T, Kume H, Adachi J, Kawasaki N, Shimizu M, Hoshino I, et al. Casein kinase 1 is recruited to nuclear speckles by FAM83H and SON. Sci Rep. 2016 Sep 29;6:34472.

27. Lebensohn AM, Dubey R, Neitzel LR, Tacchelly-Benites O, Yang E, Marceau CD, et al. Comparative genetic screens in human cells reveal new regulatory mechanisms in WNT signaling. eLife. 5:e21459.

28. Fam83h | family with sequence similarity 83, member H mouse gene | IMPC. Available from: https://www.mousephenotype.org/data/genes/MGI:2145900

29. Hagemann-Jensen M, Ziegenhain C, Sandberg R. Scalable single-cell RNA sequencing from full transcripts with Smart-seq3xpress. Nat Biotechnol. 2022;40(10):1452–7.

30. Parekh S, Ziegenhain C, Vieth B, Enard W, Hellmann I. zUMIs - A fast and flexible pipeline to process RNA sequencing data with UMIs. GigaScience. 2018 Jun 1;7(6):giy059.

31. Hao Y, Hao S, Andersen-Nissen E, Mauck WM, Zheng S, Butler A, et al. Integrated analysis of multimodal single-cell data. Cell. 2021 Jun 24;184(13):3573-3587.e29.

32. Choudhary S, Satija R. Comparison and evaluation of statistical error models for scRNA-seq. Genome Biol. 2022 Jan 18;23(1):27.

33. Ahlmann-Eltze C, Huber W. glmGamPoi: fitting Gamma-Poisson generalized linear models on single cell count data. Bioinformatics. 2021 Apr 5;36(24):5701–2.

34. Schaum N, Karkanias J, Neff NF, May AP, Quake SR, Wyss-Coray T, et al. Single-cell transcriptomics of 20 mouse organs creates a Tabula Muris. Nature. 2018 Oct;562(7727):367–72.

35. Baran-Gale J, Morgan MD, Maio S, Dhalla F, Calvo-Asensio I, Deadman ME, et al. Ageing compromises mouse thymus function and remodels epithelial cell differentiation. eLife. 2020 Aug 25;9:e56221.

36. Žuklys S, Handel A, Zhanybekova S, Govani F, Keller M, Maio S, et al. Foxn1 regulates key target genes essential for T cell development in postnatal thymic epithelial cells. Nat Immunol. 2016 Oct;17(10):1206–15.

37. Wang S, Hu Y, Yang J, Smith CE, Richardson AS, Yamakoshi Y, et al. Fam83h null mice support a neomorphic mechanism for human ADHCAI. Mol Genet Genomic Med. 2015 Sep 21;4(1):46–67.

38. Wang S, Hu Y, Smith CE, Yang J, Zeng C, Kim J, et al. The Enamel Phenotype in Homozygous Fam83h Truncation Mice. Mol Genet Genomic Med. 2019 May 6;7(6):e724.

39. Krueger A, Ziętara N, Łyszkiewicz M. T Cell Development by the Numbers. Trends Immunol. 2017 Feb;38(2):128–39.

40. Kuga T, Inoue N, Sometani K, Murataka S, Saraya M, Sugita R, et al. The conserved C-terminal residues of FAM83H are required for the recruitment of casein kinase 1 to the keratin cytoskeleton. Sci Rep. 2022 Jul 12;12(1):11819.

41. White MJ, Jacobs KA, Singh T, Mayo LN, Lin A, Chen CS, et al. Notch1 cortical signaling regulates epithelial architecture and cell–cell adhesion. J Cell Biol. 2023 Oct 5;222(12):e202303013.

42. Park JE, Botting RA, Conde CD, Popescu DM, Lavaert M, Kunz DJ, et al. A cell atlas of human thymic development defines T cell repertoire formation. Science. 2020 Feb 21;367(6480):eaay3224.

43. Balciunaite G, Keller MP, Balciunaite E, Piali L, Zuklys S, Mathieu YD, et al. Wnt glycoproteins regulate the expression of FoxN1, the gene defective in nude mice. Nat Immunol. 2002 Nov;3(11):1102–8.

44. Fujimori S, Ohigashi I, Abe H, Matsushita Y, Katagiri T, Taketo MM, et al. Fine-tuning of β-catenin in mouse thymic epithelial cells is required for postnatal T-cell development. Zúñiga-Pflücker JC, Taniguchi T, Zúñiga-Pflücker JC, Pezzano M, editors. eLife. 2022 Jan 19;11:e69088.

45. Tachie-Menson T. Investigating the role of FAM83H, a protein mutated in Amelogenesis Imperfecta.

46. Blackburn CC, Manley NR. Developing a new paradigm for thymus organogenesis. Nat Rev Immunol. 2004 Apr;4(4):278–89.

47. Boehm T. Thymus development and function. Curr Opin Immunol. 2008 Apr;20(2):178-84. doi: 10.1016/j.coi.2008.03.001. Epub 2008 Apr 9. PMID: 18403191.

48. Perez-Riverol Y, Bandla C, Kundu DJ, Kamatchinathan S, Bai J, Hewapathirana S, John NS, Prakash A, Walzer M, Wang S, Vizcaíno JA. The PRIDE database at 20 years: 2025 update. Nucleic Acids Res. 2025 Jan 6;53(D1): D543-D553. doi: 10.1093/nar/gkae1011.

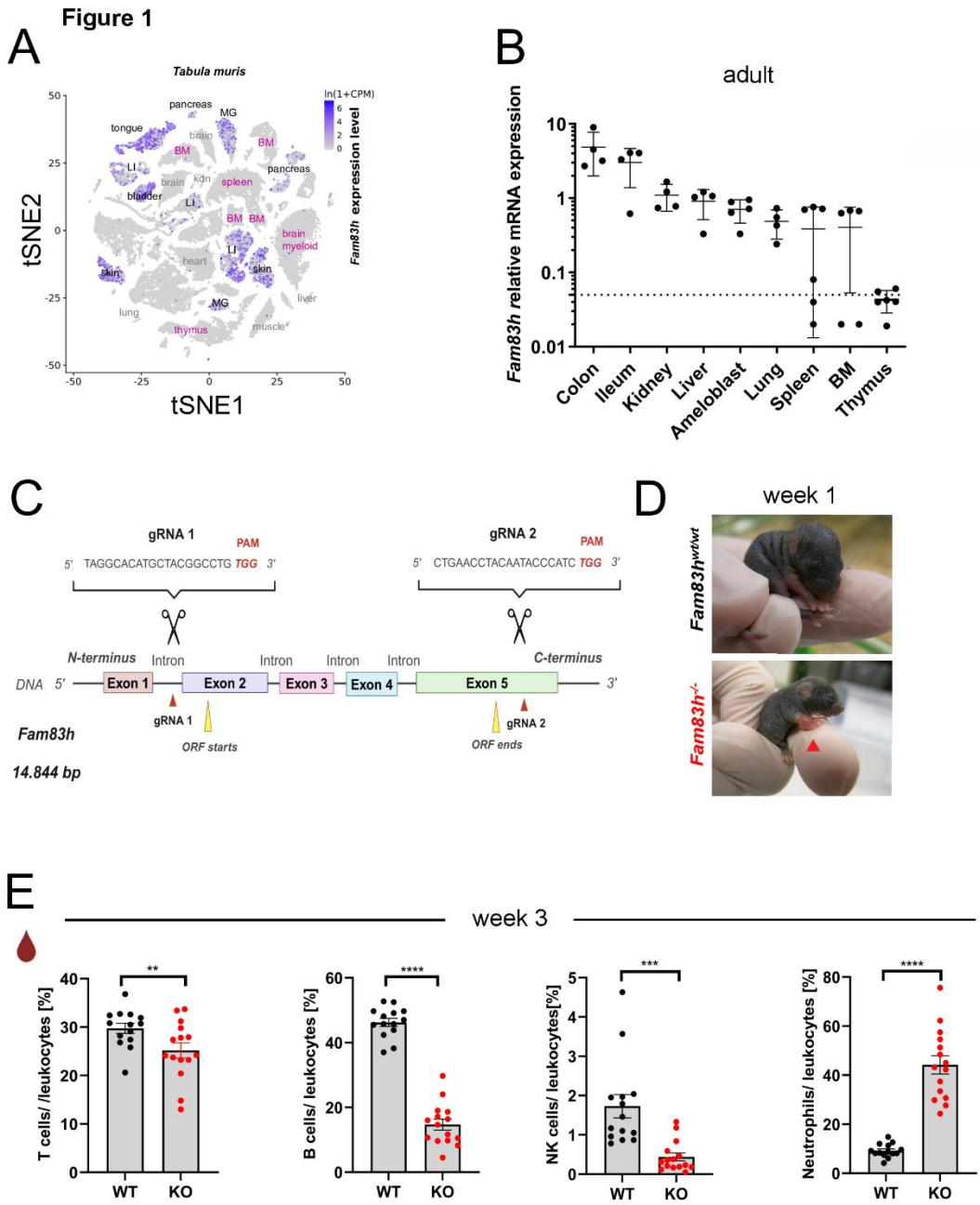

Figure 1 | *Fam83h* deficiency leads to dysregulation of early postnatal hematopoiesis and growth defects.

(A) Expression of *Fam83h* in mouse tissues (Tabula muris, *https://www.czbiohub.org/sf/tabula-muris/*).

(B) Relative mRNA expression levels of *Fam83h* in selected tissues from *Fam83h*$^{wt/wt}$ mice, normalized to the reference gene *Casc3* (RT-qPCR). Symbols indicate individual mice. Data are presented as mean ± SD, *n*=4 in GraphPad (version 9).

(C) Generation of *Fam83h*$^{-/-}$ mice – Schematic representation of the CRISPR/Cas9-mediated knockout strategy for *Fam83h*, targeting regions upstream of exon 2 and within exon 5 using two sgRNAs is depicted (created by BioRender).

(D) By postnatal week 1, *Fam83h*$^{-/-}$ mice exhibit forepaw swelling compared to *Fam83h*$^{wt/wt}$ littermates.

(E) At postnatal week 3, *Fam83h*$^{-/-}$ mice show altered hematopoietic profiles in peripheral blood, assessed by flow cytometry (FCM). The gating strategy is depicted in Figure S7. The graph represents 6 independent experiments. Symbols denote individual mice, with bars indicating mean ± SEM, unpaired *t-test*, p-values: **P ≤ 0.01, ***P ≤ 0.001, ****P ≤ 0.0001.

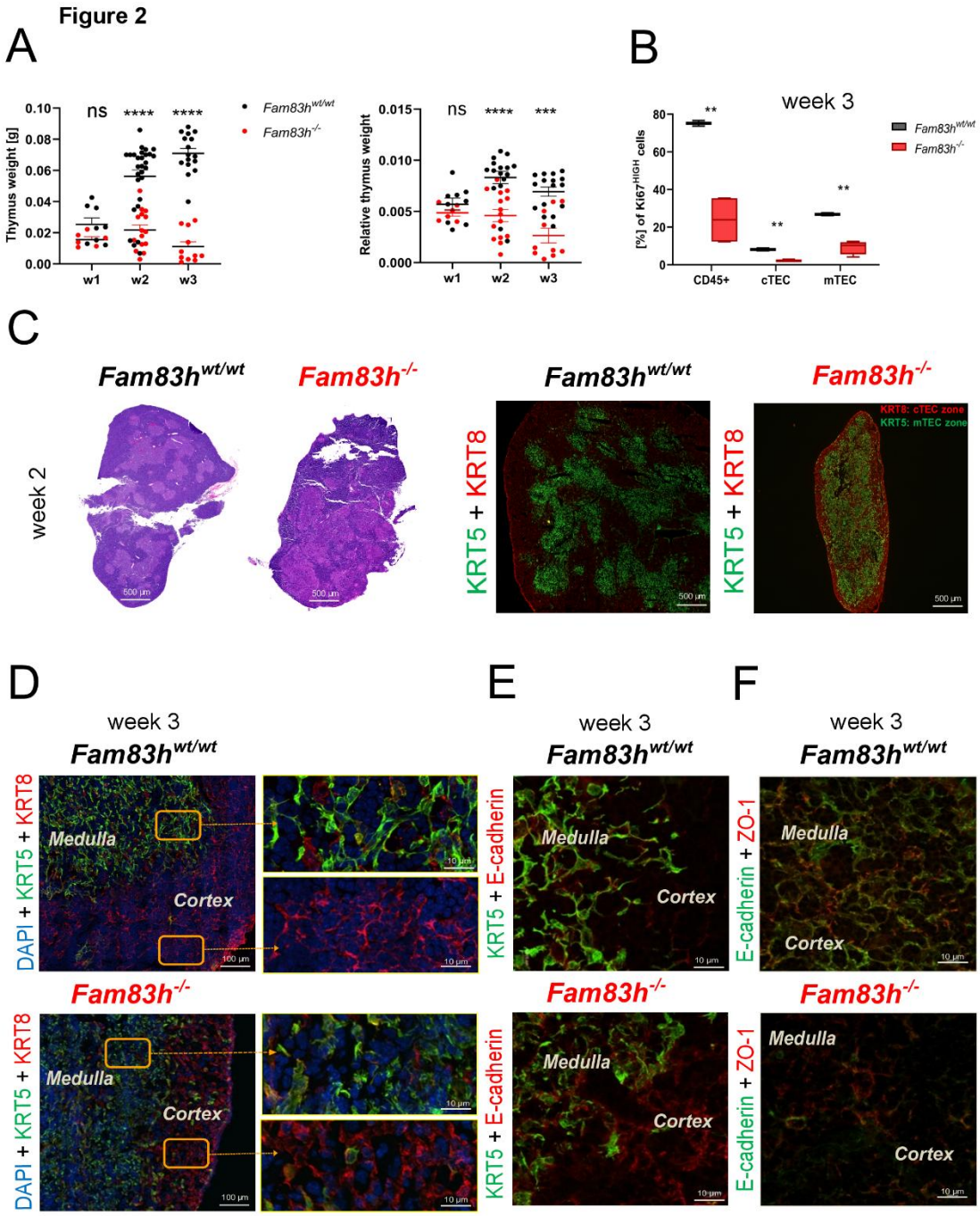

Figure 2 | *Fam83h* deficiency leads to altered thymic architecture in early-postnatal thymus.

(A) Thymus weight and relative thymus-to-body weight ratio were assessed at weeks 1, 2, and 3. The graph represents 3 independent experiments for week 1, 11 for week 2, and 6 for week 3. Symbols indicate individual mice, mean ± SEM, p-values: ns (P > 0.05), ***P ≤ 0.001, ****P ≤ 0.0001.

(B) The proportions of proliferating, Ki67HIGH cells within the TEC and thymic CD45^{+} populations were measured by FCM (for gating hierarchy see Figure S16 at week 2–3 of age, *n*=2 for *Fam83h*$^{wt/wt}$ and *n*=4 for *Fam83h*$^{-/-}$, unpaired *t-test (box and whiskers, median/ min to max)*, p-values: **p ≤ 0.01.

(C) Hematoxylin and Eosin (H&E) staining. Scale bar = 500 µm and immunofluorescence (IF) staining of week 2-3 old thymi. Double staining for keratin-8 (cTEC, red) and keratin-5 (mTEC, green) enables distinguishing cortical (red) and medullary (green) areas. H&E and IF were imaged by brightfield and widefield fluorescence microscopy. Scale bar = 500 µm. Representative images from 3 independent experiments.

(D) Cryosections from week 3 old *Fam83h*$^{wt/wt}$ *and Fam83h*$^{-/-}$ thymi were stained for keratin-5 (green) and keratin-8 (red) were imaged by spinning disk confocal microscopy (SDCM). DAPI staining marks nuclei (blue), aiding in cortex-medulla distinction. Representative images from 3 independent experiments. Scale bar = 100 µm and 10 µm.

(E) Cryosections from week 3 old *Fam83h*$^{wt/wt}$ *and Fam83h*$^{-/-}$ thymi were stained for E-cadherin (red) and keratin-5 (mTEC, green), analyzed using SDCM. Scale bar = 10 µm.

(F) Cryosections from week 3 old *Fam83h*$^{wt/wt}$ *and Fam83h*$^{-/-}$ thymi were stained for ZO-1 (red) and E-cadherin (green), analyzed using SDCM. Scale bar = 10 µm.

Figure 3

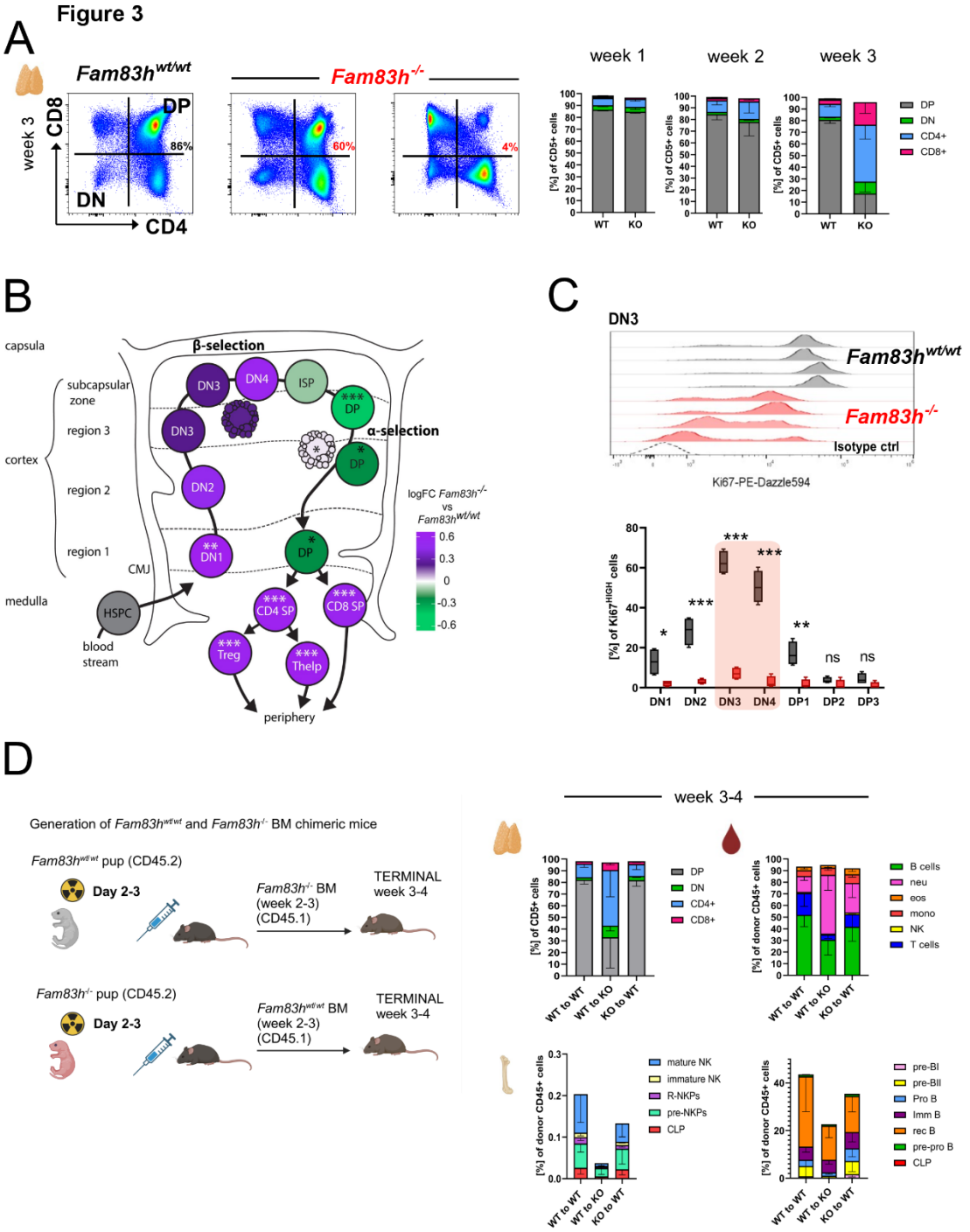
A
Fam83h wt/wt
Fam83h -/-
week 3
CD8
CD4
DP
DN
86%
60%
4%
week 1
week 2
week 3
[%] of CD5+ cells
WT
KO
DP
DN
CD4+
CD8+
B
capsula
subcapsular zone
region 3
cortex
region 2
region 1
medulla
CMJ
β-selection
α-selection
DN3
DN4
ISP
DP
DN2
DN1
HSPC
blood stream
CD4 SP
CD8 SP
Treg
Thelp
periphery
logFC Fam83h -/- vs Fam83h wt/wt
0.6
0.3
0
-0.3
-0.6
C
DN3
Fam83h wt/wt
Fam83h -/-
Isotype ctrl
Ki67-PE-Dazzle594
[%] of Ki67 HIGH cells
DN1
DN2
DN3
DN4
DP1
DP2
DP3
ns
D
Generation of Fam83h wt/wt and Fam83h -/- BM chimeric mice
Fam83h wt/wt pup (CD45.2)
Day 2-3
Fam83h -/- BM (week 2-3) (CD45.1)
TERMINAL week 3-4
Fam83h -/- pup (CD45.2)
Fam83h wt/wt BM (week 2-3) (CD45.1)
week 3-4
[%] of CD5+ cells
[%] of donor CD45+ cells
WT to WT
WT to KO
KO to WT
B cells
neu
eos
mono
NK
T cells
mature NK
immature NK
R-NKPs
pre-NKPs
CLP
pre-BI
pre-BII
Pro B
Imm B
rec B
pre-pro B

Figure 3 | Thymocyte development is impaired in *Fam83h*$^{-/-}$ animals.

(A) FCM analysis of the main thymocyte subsets: DN (green), DP (gray), CD4^{+} SP (blue), and CD8^{+} SP (magenta) at different time points (week 1, week 2, and week 3). The gating strategy is shown in Figure S10. Bars represent mean ± SD. Data are based on 3 independent experiments, *n*=9 for *Fam83h*$^{wt/wt}$ and *n*=7 for *Fam83h*$^{-/-}$ (week 1), *n*=11 for *Fam83h*$^{wt/wt}$ and *n*=6 for *Fam83h*$^{-/-}$ (week 2), and *n*=8 for *Fam83h*$^{wt/wt}$ and *n*=6 for *Fam83h*$^{-/-}$ (week 3).

(B) Schematic representation (Modified from (46)) of developmental blocks in T cell development in *Fam83h*$^{-/-}$ animals based on FCM analysis of week 3 old thymi (Figure S10). LogFC *Fam83h*$^{-/-}$ vs *Fam83h*$^{wt/wt}$ is shown for each T cell stage.

(C) Proliferation was determined by FCM analysis of Ki67 levels in thymocyte subsets (Figure S11). Representative histograms showing the decrease of Ki67 expression in *Fam83h*$^{-/-}$ (red) as compared to *Fam83h*$^{wt/wt}$ (gray) DN3 thymocytes at week 2-3 of age. The isotype control signal is depicted by the dashed line. The plot below shows the quantification of Ki67 staining in DN1–DP3 T cell subsets. Data are presented as min-max normalized percentages, *n*=4 for *Fam83h*$^{wt/wt}$ and *n*=4 for *Fam83h*$^{-/-}$, unpaired *t-test*, p-values: ns (P > 0.05), *P ≤ 0.05, **P ≤ 0.01, ***P ≤ 0.001.

(D) Schematic diagram illustrating the generation of *Fam83h*$^{-/-}$ and *Fam83h*$^{wt/wt}$ BM chimeras. FCM analysis of thymus (upper middle panel, Figure S12) and blood (upper right panel, Figure S13) and bone marrow (lower middle and right panels, Figure S14) was performed at week 3–4 post-BM transfer to assess the contribution of donor-derived hematopoietic stem cells (HSCs) to the main hematopoietic lineages. Quantification of DN (green), DP (gray), CD4^{+} SP (blue), and CD8^{+} SP (magenta) thymocytes (Middle panel) and hematopoietic lineages in the peripheral blood. Data are based on 5 independent experiments, *n*=7 from *Fam83h*$^{wt/wt}$ to *Fam83h*$^{wt/wt}$, *n*=7 from *Fam83h*$^{wt/wt}$ to *Fam83h*$^{-/-}$, *n*=12 from *Fam83h*$^{-/-}$ to *Fam83h*$^{wt/wt}$ (blood), *n*=12 from *Fam83h*$^{wt/wt}$ to *Fam83h*$^{wt/wt}$, *n*=4 from *Fam83h*$^{wt/wt}$ to *Fam83h*$^{-/-}$, *n*=16 from *Fam83h*$^{-/-}$ to *Fam83h*$^{wt/wt}$ (thymus). Bars indicate mean ± SD. Development of B and NK cells in the BM of reciprocal BM chimeras. Frequencies of B and NK cell progenitors in donor-derived BM were determined at week 3–4 post-transplantation. Bars indicate mean ± SD. Sample sizes: for B cells, *n*=4, 7, 9 for WT→WT, WT→KO, and KO→WT groups, respectively; for NK cells, *n*=3, 7, 6 for WT→WT, WT→KO, and KO→WT groups, respectively (NK; natural killer, R-NKP; refined natural killer progenitors).

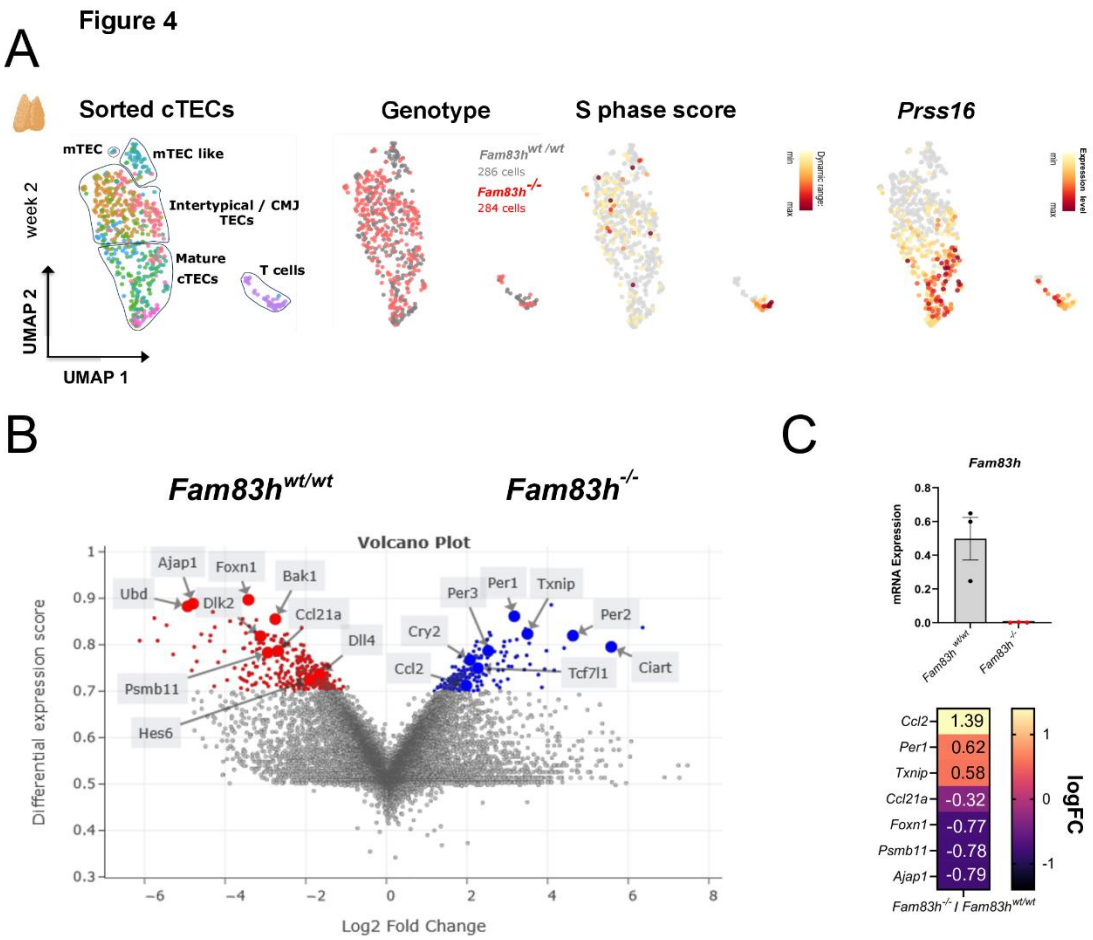

Figure 4 | *Fam83h* deficient cTECs fail to express *Foxn1* and its target genes.

(A) EpCAM+UAE-Ly51+ cTECs were single-sorted (Figure S15) from *Fam83h*$^{wt/wt}$ and *Fam83h*$^{-/-}$ thymi at 2 weeks of age and processed by sc-RNAseq using Smart-seq technology (29) UMAP projection shows 570 cells that passed quality control. Leiden clusters were identified using the Scarfweb platform and manually annotated (far left panel). UMAP projections show an overlay of *Fam83h*$^{wt/wt}$ (gray, 286 cells) and *Fam83h*$^{-/-}$ (red, 284 cells) cells (left panel), S phase score (right panel), and cTEC marker gene, *Prss16*, expression level (far right panel).

(B) Genes differentially expressed by mature cTECs isolated from *Fam83h*$^{wt/wt}$ and *Fam83h*$^{-/-}$ thymi.

(C) RT-qPCR analysis of mRNA expression of selected genes in *Fam83h*$^{wt/wt}$ and *Fam83h*$^{-/-}$ cTECs. Relative *Fam83h* expression, normalized to the *Cas3* reference gene, is shown in the upper panel. Data are presented as mean ± SEM and represent 2 to 3 independent experiments. The heatmap displays median expression values.

Figure 5

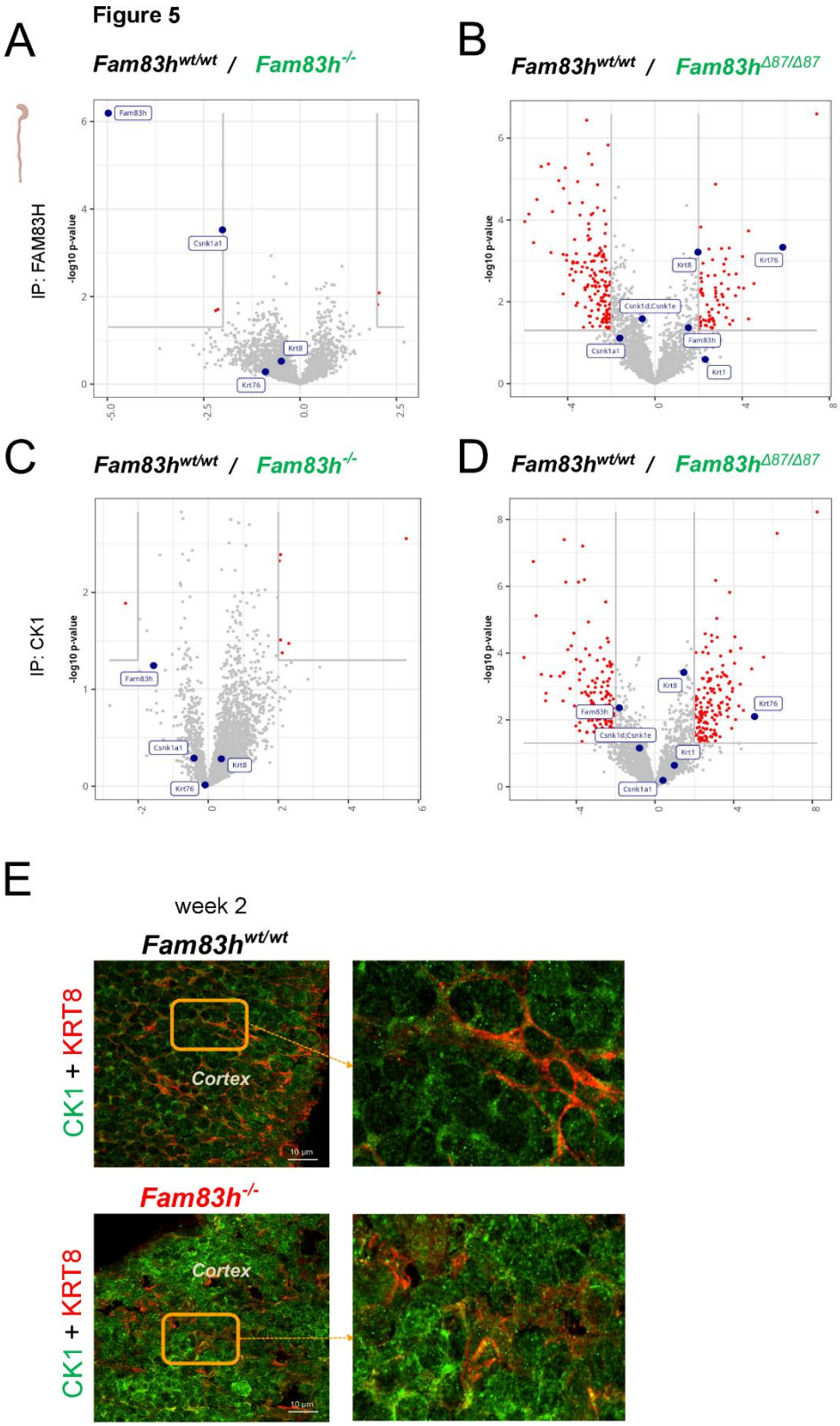
A
Fam83h^wt/wt / Fam83h^-/-
IP: FAM83H
-log10 p-value
Fam83h
Csnk1a1
Krt8
Krt76
B
Fam83h^wt/wt / Fam83h^Δ87/Δ87
Krt8
Krt76
Csnk1d;Csnk1e
Fam83h
Csnk1a1
Krt1
C
Fam83h^wt/wt / Fam83h^-/-
IP: CK1
Fam83h
Csnk1a1
Krt8
Krt76
D
Fam83h^wt/wt / Fam83h^Δ87/Δ87
Krt8
Fam83h
Krt76
Csnk1d;Csnk1e
Krt1
Csnk1a1
E
week 2
Fam83h^wt/wt
CK1 + KRT8
Cortex
10 µm
Fam83h^-/-
CK1 + KRT8
Cortex
10 µm

Figure 5 | Mass spectrometry analysis of FAM83H and CK1 interacting proteins in ileum tissue from *Fam83h$^{wt/wt}$, Fam83h$^{-/-}$,* and *Fam83h$^{\Delta 87/\Delta 87}$ confirms that Fam83h$^{\Delta 87/\Delta 87}$* fails to interact with CK1a.

(A-D) Mass spectrometry was performed on ileum lysates immunoprecipitated from *Fam83h$^{wt/wt}$*, *Fam83h$^{-/-}$*, and *Fam83h$^{\Delta 87/\Delta 87}$* samples using anti-CK1 and anti-FAM83H antibodies. The analysis aimed to identify FAM83H and CK1-associated proteins and compare their abundance between *Fam83h$^{wt/wt}$* and Fam83h deficient (*Fam83h$^{-/-}$*) (A, C) and *Fam83h truncated (Fam83h$^{\Delta 87/\Delta 87}$) samples (B, D).* Data represents 5 *Fam83h$^{wt/wt}$,* 4 *Fam83h$^{-/-}$* and 6 *Fam83h$^{\Delta 87/\Delta 87}$.*

(E) Cryosections from week 2 old *Fam83h$^{wt/wt}$ and Fam83h$^{-/-}$* thymi were stained for CK1 (green) and keratin-8 (red) were imaged by SDCM. Representative images from 3 independent experiments. Scale bar = 10 µm.